Korean J. Chem. Eng., 35(3), 684-693 (2018)
DOI: 10.1007/s11814-017-0299-3

pISSN: 0256-1115
eISSN: 1975-7220

Binary semiconductor oxide nanoparticles on graphene oxide (CdO/CeO_2/RGO) for the treatment of hazardous organic water pollutants

Hoda Mirzazadeh and Maryam Lashanizadegan†

Department of Chemistry, Faculty of Physics & Chemistry, Alzahra University, P. O. Box 1993893973, Tehran, Iran
(*Received 29 July 2017 • accepted 22 October 2017*)

Abstract−CdO/CeO_2/RGO was prepared by a hydrothermal process. The physical properties of CdO/CeO_2/RGO have been investigated by FTIR, XRD, DRS, TEM, SEM and EDX. CdO/CeO_2/RGO was used for sonocatalytic degradation of Ibuprofen (IBP), Rodamin B (RhB) and Methyl orange (MO) under ultrasonic irradiation. The catalytic properties of CdO/CeO_2/RGO were evaluated with the reduction of 4-nitrophenol (4-NP) into 4-aminophenol (4-AP) by $NaBH_4$. The highest degradation efficiency of IBP in presence of $K_2S_2O_8$ (91%), RhB (97%) and MO (85%) was observed within 80, 150 and 150 min after the beginning of the reaction, respectively. The reduction efficiency of 4-NP was 79% within reaction time of 70 min. Compared to the reduced graphene oxide (RGO) and CdO/CeO_2 nanoparticles, CdO/CeO_2/RGO exhibits excellent sonocatalysis on degradation of IBP, azo dyes and catalysis activity on reduction of 4-NP.

Keywords: Sonocatalysis, Catalytic, 4-Nitrophenol, Degradation, Reduction, Azo Dyes, Ibuprofen

INTRODUCTION

Different industries like pharmaceutical, textile, paper, cosmetics, leather and so on discharge effluents containing large amounts of aromatic compounds and dyes in water [1,2]. NSIDS (non-steroidal anti-inflammatory drugs), aromatic compounds and azo dyes are toxic to the health and life of all living organisms. So it is necessary to separate and purify these toxic compounds from wastewater before discharging it into the environment [3-7]. IBP as a common NSIDS is used for treating pain, fever and inflammation [8-10]. 4-NP is a kind of dangerous substrate in many chemicals and drug industries; it can invade the body through respiratory and digestive systems [5]. Azo dyes like MO and RhB are toxic with known harmful effects on humans. Of most of the techniques applied to reduce 4-NP and degradation of IBP, azo dyes have disadvantages such of sludge generation and membrane fouling. Recent studies justify using catalysts that can be regenerated or reused multiple times without any significant dye removal change in efficiency. Sonocatalytic technology is one of the newest methods that can help in reduction and degradation of toxic compounds [11-13]. Due to importance of 4-AP in applications like photographic developer, dyeing agent, inhibiting agent, etc., the reduction reaction of 4-NP to 4-Amino phenol (4-AP) by $NaBH_4$ is notable [14,15]. Therefore, a cheaper and more efficient method for catalytic reduction of 4-NP is always in demand. In the past, a large variety of catalysts have been used for this reduction. Zhang et al. reported using Ag nanoparticles within the pores of mesoporous silica [16]. Liu et al. used layered alumina silicate nano tubes to encapsulate Ag nanoparticles [17]. Saraschandre et al. used silver doped TiO_2 as catalyst [18]. There are many examples for degradation of IBP, MO and RhB with different catalysts. For example, Hianese et al. studied IBP degradation by UV light [19]. Lei et al. investigated photocatalytic degradation of ibuprofen in aqueous solution using novel visible-light responsive graphene quantum dot/$AgVO_3$ nanoribbons [20]. Li et al. reported using TiO_2/graphene composite and ultrasonic waves to reduce the rhodamine dye [21]. Ahmad et al. investigated the degradation of RhB as a dye pollutant in the presence of pristine ZnO nanoparticles and ZnO/CNTs composites using sonocatalysis systems [22]. Tangavel et al. produced GO-Fe^{3+} hybrid nanosheets with catalytic properties for reducing the red color code 120 using ultrasound [23]. Saharan et al. focused on the synergistic effect of Ni doped ZnO nanoparticles and ultrasonication for the degradation of dyes [24]. However, there are very few reports about catalysts that can be applied in both catalytic and sonocatalytic reactions.

Cerium oxides are another group of effective catalysis in oxidation of organic materials, such as phenols and cyclohexene [25]. Also effective for dye removal, they have large pore size that can easily accommodate dye molecules [26] Cerium oxides can improve the efficiency of catalyst after being composited with other semiconductors [27]. CdO is an important semiconductor that can be potentially applied in many fields, such as solar cells, photocatalysts, and catalysts [28] The composition of CdO and CeO_2 could not only effectively expand the absorption range, but also favors the separation of electron-hole pairs for their energy level structure matching very well.

Graphene, as a two-dimensional carbon nanomaterial, has been used for high mobility, chemical stability due to its unique structure. The coupling of graphene with some semiconductors has shown a significant improvement of catalytic ability for superior charge transport properties [29-32]. The present research work is about preparation of CdO/CeO_2 nanoparticles on graphene layers using modified Hummers method and hydrothermal process. The process was quite simple and presented good repeatability. CdO/

†To whom correspondence should be addressed.
E-mail: m_lashani@alzahra.ac.ir, mlashani@hotmail.com

CeO_2/RGO was selected as sonocatalyst for removal of IBP and azo dyes from wastewater. Furthermore the reduction reaction of 4-NP to 4-AP by $NaBH_4$ is discussed.

EXPRIMENTAL SECTION

1. Instruments and Reagents

All materials were commercial reagent grade. FT Infrared (FT-IR) spectra were obtained as potassium bromide pellets in the range of 400-4,000 cm^{-1} with a Bruker tensor 27DTGS. UV-Vis spectra were recorded on Lambda 35 spectrophotometer. XRD pattern was recorded by Jeol JDX-8030 with Cu k_α radiation (λ=1.54 Å) in the range of 2θ=10-80°. The morphology, particle size, elements distribution and energy dispersive spectroscopy (EDS) of samples were observed by a scanning electron microscopy (SEM, KYKY-EM3200) and transmission electron microscope (Zeiss-EM10C-(100 KV) German). Ultrasonic experiments were done on an ultrasonic processor, VCX 750 USA, ultrasonic frequency 20 kHz and output power of (500W-1200W) through manual adjusting. Diffuse reflectance spectroscopy (DRS) was carried out on Avantes (Ava Lamp-DH-S Ava spec2048-Tec)

2. Synthesis of Materials

2-1. Preparation of Mixture CdO/CeO_2 Nanoparticles

Four (4) mL of 0.5 M solution of $Ce(NO_3)_3{\cdot}6H_2O$ and 4 mL of 0.5 M solution of $Cd(CH_3COO)_2{\cdot}2H_2O$ were added to a conical flask containing a mixed solution of 50 mL distilled water, 2.8 g NaOH, 10 mL of PEG (M_w=400), blended well by stirring for 15 min at 70 °C. The mixed solution was left for four days at room temperature. White crystalline products were collected, centrifuged, washed with distilled water and ethanol several times and dried at 60 °C in an oven, then calcined at 400 °C for 1 h [33].

2-2. Preparation of Graphene Oxide (GO)

GO was synthesized from purified natural graphite powder via a modified Hummers method [34]. Briefly, 1.0 g of graphite powder and 0.5 g of $NaNO_3$ were added to 48 mL of concentrated H_2SO_4 solution within an ice bath. Under intense stirring, 3 g of $KMnO_4$ was gradually added to the above solution, and the temperature was maintained below 20 °C. Then the above mixture was vigorously stirred at 35 °C for 18 h in a water bath. After the reaction was completed, 75 mL of deionized water was slowly added to the above system in an ice bath with the temperature below 50 °C. Then, 5 mL of 30% H_2O_2 dissolved in 120 mL of deionized water was added, and the solution was continuously stirred for another 2 h. The product was washed with 120 mL of 10% HCl aqueous solution, followed by washing with deionized water and ethanol to remove other ions. Finally, the resulting material was dried at 60 °C in an oven.

2-3. Preparation of CdO/CeO_2/RGO

In a typical process to synthesize CdO/CeO_2/RGO, 0.2 g of graphene oxide was dispersed in 30 mL of deionized water by sonication for 1 h. Under vigorous stirring, 20 mL of deionized water containing 0.02 g CdO/CeO_2 was slowly added into the GO suspension. After stirring for 1 h, 20 mL of $N_2H_4{\cdot}H_2O$ was added into the above system and then the solution was sealed in a 100 mL Teflon-lined stainless steel autoclave for hydrothermal reaction at 180 °C for 8 h. After the autoclave was cooled to room temperature naturally, CdO/CeO_2/RGO product was collected, washed with water for several times, and dried at 60 °C in an oven for 10 h. The obtained sample was denoted as CdO/CeO_2/RGO 10% wt CdO/CeO_2/RGO 20% wt and CdO/CeO_2/RGO 30% wt were synthesized by feeding 0.04 and 0.06 g of CdO/CeO_2 nanoparticles, respectively. RGO was synthesized under the same condition in the absence of CdO/CeO_2 nanoparticles.

3. Applying CdO/CeO_2/RGO as Catalyst in Catalytic and Sonocatalytic Reactions

3-1. Adsorption and Sonocatalytic Study

All the organic pollutants experiments were conducted in 50 mL beakers. 25 mL of IBP, RhB and MO (20 mg/L) containing 1.2 g/L catalyst were prepared. All of the solutions except IBP solution were prepared with deionized water. The IBP solution was prepared in methanol as solvent. 1 mL $K_2S_2O_8$ (0.5 mmol/L) was added to IBP solution. The reaction mixture was placed in dark ambiance. To study adsorption effect, the mixture solutions were magnetically stirred in darkness to reach the adsorption/desorption equilibrium for 30 min. The ultrasonic probe was operated at a fixed frequency of 20 kHz, with an output power of 1,200 W through manual adjustment. The ultrasonication temperature was set to be 25 °C all through the experiments. The water bath was used in keeping the temperature under control, at around 25 °C. After 30 min, using ultrasonic apparatus, at different time intervals, 1 mL of reaction mixture was withdrawn from the reaction mixture and the concentration of IBP, MO and RhB was measured. The calculations of the absorption spectra were carried out at 465 nm for MO, 555 nm for RhB and 223 nm for IBP, which were found to be wavelengths at which the highest peaks of absorbance of the organic pollutants were obtained (λ_{max}).

3-2. Determination the Kind of ROS

Three 5 mL DPCI solution (10^{-2} M) were added into three volumetric flasks marked as a-c, respectively. And then 1.2 g/L of CdO/CeO_2/RGO was added to each one. 2.5 mL of {(L-His, Thiourea and Vitamin C (VC)) 5×10^{-3} M} added into (a)-(c) flasks, respectively. All solutions were diluted to 25 mL with double distilled water. Any of the solution was transferred into two conical flasks. Then one of the conical flasks was placed under ultrasonic irradiation, and the other one was stored under stirring. After 45 min, from each sample 10 mL solution was taken and extracted with benzene-tetrachloride carbon (volume ratio=1 : 1); then the UV-Vis spectra of all solutions were obtained.

3-3. Catalytic Study

First, 2 mL $NaBH_4$ (0.1 M) solution (freshly prepared), 1.2 g/L catalyst were mixed with 100 mL deionized water. For starting the reaction, 2 mL 4-NP (5 mM) solution was added to mixture solution at room temperature (~25°). During the reaction process, 1 mL of the reaction mixture was taken from reaction system at certain time intervals, followed by the recording of the UV-Vis spectra of the solution to test the concentration of 4-NP by monitoring the absorption peak at 400 nm.

RESULTS AND DISCUSSION

1. Characterization

The X-ray diffraction (XRD) patterns of GO, RGO and CdO/

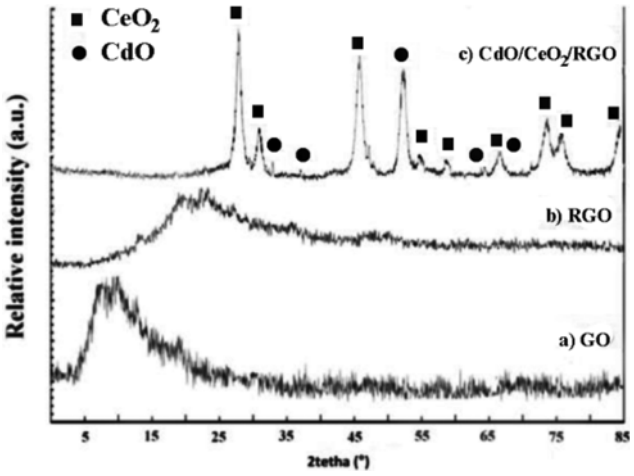

Fig. 1. XRD pattern of (a) GO, (b) RGO and (c) CdO/CeO_2/RGO.

CeO_2/RGO are shown in Fig. 1. The XRD pattern of GO shows a peak at 2θ=10.3°. It can be indexed to (002) crystallographic plane of GO [35,36]. In the XRD pattern of RGO nanosheets, the disappearance of the peak at 2θ=10.3° confirms that the graphite oxide has been flaked to GO [37]. Also, RGO exhibited a broad peak at 24.6° which corresponds to (002) plane. Fig. 1(c) shows characteristic peaks at 2θ=28.8°, 32.6°, 47.7°, 56.7°, 59.0°, 69.1°, 77.3°, 79° and 89.5°, which can be indexed to (111), (200), (220), (311), (222), (400), (331), (420) and (420) planes of cubic structured CeO_2 (JCPDS no. 81-0792). The peaks around 33.2°, 38.6°, 55.7°, 66.5°, 69.2° can be indexed to (111), (200), (202), (311) and (222) planes of cubic structure of CdO(JCPDS no. 65-2908). No diffraction peak corresponding to RGO was observed in the XRD pattern of CdO/CeO_2/RGO. It is speculated that CdO/CeO_2 nanoparticles growth between interlayer of rGO sheet led to exfoliation of rGO. Earlier studies showed exfoliation of rGO can cause their diffraction peaks to become weak or even disappear [21,34]. The XRD pattern of CdO/CeO_2/RGO indicates that the synthesized nanocomposite is highly crystalline.

The surface morphology and particle size of CdO/CeO_2/RGO were analyzed by SEM images (Fig. 2). As shown in Fig. 2(a) CdO/CeO_2 nanoparticles have regular shaped morphology. They are aggregated as seen from the SEM images. The particles have estimated size ranging 20 and 30 nm. Fig. 2(b) indicates CdO/CeO_2 nanoparticles were distributed as homogeneous particles on graphene sheet. The elemental composition was analyzed by an energy dispersive spectrometer (EDS) spectrum equipped with the SEM. The peaks associated with carbon (40.9%), cerium (24.9%), cadmium (14.5%) and oxygen (19.7%) are observed in Fig. 2(c). The presence of these elements on CdO/CeO_2/RGO is the main constituent for catalytic activity of the nanocomposites.

The TEM images of CdO/CeO_2/RGO (20% wt) are shown in Fig. 3(a), (b). As can be seen, the CdO/CeO_2 nanoparticles are distributed on the surface of RGO. The nanocomposites exhibit uniform particle sizes. The presence of reduced graphene oxide leads to a lower aggregation of the nanoparticles. From TEM images it is deduced that there is a reasonably strong interaction between CdO/CeO_2 nanoparticles and RGO, otherwise these nanoparticles would aggregate. Moreover, the TEM image clearly shows that the particles are dispersed homogeneously and have good agreement with the results given by XRD, SEM and EDX.

The FTIR spectrum of the as-synthesized GO confirms the

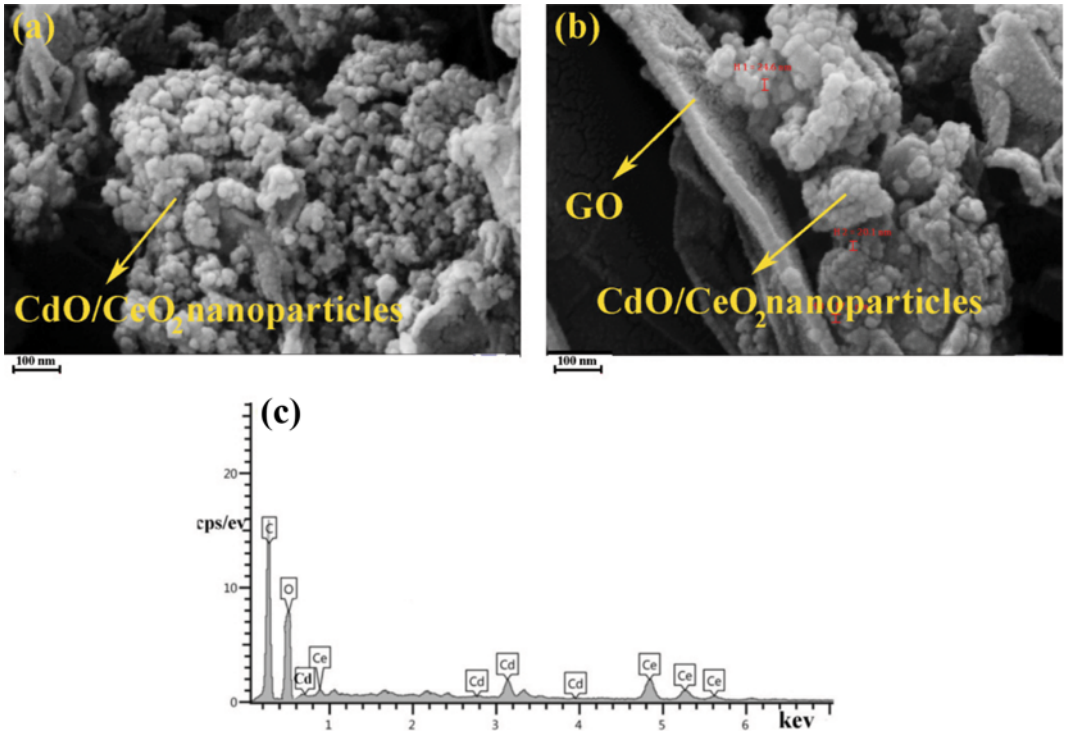

Fig. 2. SEM images of CdO/CeO_2/RGO with different magnifications (a), (b), (c) EDX spectrum of CdO/CeO_2/RGO.

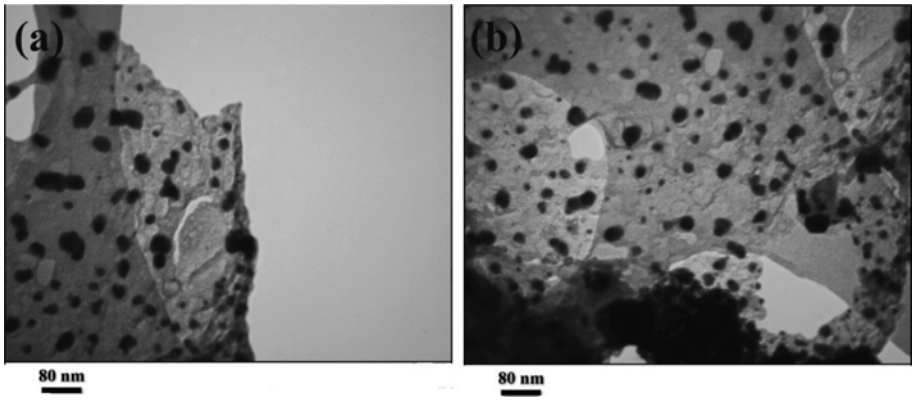

Fig. 3. TEM images of CdO/CeO_2 nanoparticles on reduced graphene oxide with different magnification (a), (b).

successful oxidation of graphite. In detail, the absorption band at 3,400 cm^{-1} originates from stretching vibration of O-H. Stretching vibration peaks of C=O, C=C, C-O-C and C-O are observed at 1,730, 1,672, 1,170 and 1,044 cm^{-1}, respectively. The FTIR spectrum of the RGO shows absorption band at 1,635 cm^{-1} due to the C=C stretching vibration. The reduction of GO was confirmed from disappearance of the absorption peak at 1,060 cm^{-1} and reduction of the absorption at 1,720, 1,170 cm^{-1}. In the FTIR spectrum of CdO/CeO_2/RGO, a characteristic peak at 1,635 cm^{-1} has observed. The absorption at 1,720, 1,170 cm^{-1} has decreased and the absorption at 1060 has vanished. The presence of CdO/CeO_2 nanoparticles in CdO/CeO_2/RGO is ensured from the bands observed at 464 and 520 cm^{-1} owing to the Cd-O and Ce-O stretching mode, respectively [31,36]. The decreasing oxygen containing groups (C=O and C-O-C) and vanishing (C-O) in the FTIR spectra of CdO/CeO_2/RGO could provide enough adhesion strength to inhibit the aggregation and loss of CdO/CeO_2 nanoparticles during sonocatalytic process and excellent stability (Fig. S1 in supplementary material) [38].

2. Adsorption Properties of the As-prepared Nanocomposites

From Fig. S2, after 30 min 27% of IBP, 23% of RhB and 30% of MO were adsorbed. By the observations it was clear that after 30 min, the absorption spectrum of the organic pollutants reached almost constant value. The percentage of the organic pollutant degradation (Deg %) was calculated as follows:

$$\text{Deg } \% = \left(\frac{C_0 - C_f}{C_0}\right) \times 100 \quad (1)$$

where C_0 and C_f are the initial and final organic pollutants concentrations, respectively.

3. Sonocatalytic Properties of CdO/CeO_2/RGO

Fig. 4(a)-(c) shows UV-Vis absorption spectrums of MO, IBP and RhB in the presence of ultrasonic and CdO/CeO_2/RGO as catalyst. A significant regular reduction in the intensity of the absorption peak of azo dyes and IBP is observed after 150 and 80 min at the beginning of reaction, respectively. To compare different factors that are important in degradation process, some experiments were carried out. As can be seen in Fig. 4(d), 24% of RhB, 25% of MO and 31% of IBP were degraded in presence of only ultrasonic waves (without CdO/CeO_2/RGO). The CdO/CeO_2 nanoparticles have the ability to remove 39% of RhB, 44% of MO and 48% of IBP in presence ultrasonic waves. The RGO alone with ultrasonication can degrade 42% of RhB, 48% of MO and 51% of IBP. The results demonstrate excellent removal efficiency was achieved in presence of CdO/CeO_2/RGO and ultrasonication (RhB: 97%, MO: 85% and IBP: 91%). Also, the change in concentration of MO, IBP and RhB is shown in Fig. 4(e). A notable decrease in concentration of IBP, MO and RhB can be seen with increasing time intervals in the presence of ultrasonic and CdO/CeO_2/RGO. It is found that unique properties of RGO, being more conductive than GO, provides a high surface area support for immobilization of CdO/CeO_2 nanoparticles, thus favoring the degradation due to synergistic interaction between CdO/CeO_2 and RGO.

4. Optimizing Combination Ratio of CdO/CeO_2 to RGO

Series ratios of CdO/CeO_2 to RGO were prepared (CdO/CeO_2/RGO 10% wt, CdO/CeO_2/RGO 20% wt and CdO/CeO_2/RGO 30% wt). The prepared composites were applied in degradation of IBP as a model reaction and the degradation ratio was calculated with C_t/C_0, where C_0 is the initial concentration and C_t is the concentration of IBP at different times. Fig. 5 shows the time profile of C_t/C_0 using the main absorption peak of IBP (223 nm in Fig. 4). As evident in Fig. 5, CdO/CeO_2/RGO (10% wt), CdO/CeO_2/RGO (20% wt) and CdO/CeO_2/RGO (30% wt) samples exhibited improved sonocatalytic activity when compared to CdO/CeO_2 nanoparticles and RGO. Also, Fig. 5 indicates the highest degradation efficiency was achieved in presence of CdO/CeO_2/RGO (20% wt).

5. Effect of pH

The effect of pH on the degradation efficiency of IBP, MO and RhB was examined in the range 4-12 in an aqueous solution in the presence of CdO/CeO_2/RGO. Fig. 6 demonstrates the highest degradation efficiency of IBP was at pH=4. Pharmaceuticals exist in neutral form hydrophobic at pH below pK_a, but in anionic form (hydrophilic) at pH above pK_a [39]. IBP exist in neutral form at pH=4 (pK_a=5.4); at pH higher than pK_a, the dissociation of hydrogen ion from the IBP results in a negatively changed IBP anion, also in pH higher than 7, higher amount of OH^- is produced, which leads to an electrostatic repulsion. Another reason for the inhibited degradation at high pH is the self-dissociation of $^{\bullet}SO_4^-$; thus the fewer sulfate radicals are available for IBP degradation [40]. Consequently, the degradation efficiency of IBP is decreased. Therefore, the optimum pH for IBP degradation is 4. MO has a

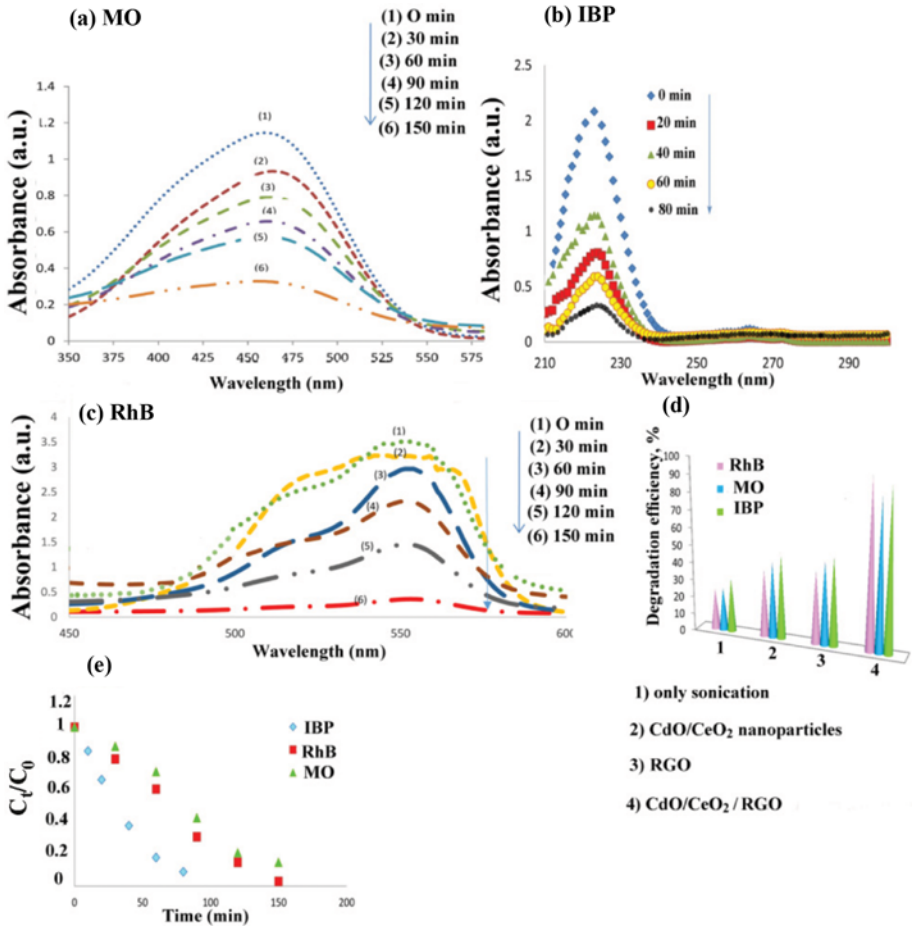

Fig. 4. (a)-(c) UV-vis spectra of MO, IBP and RhB at different time intervals in presence ultrasonic and CdO/CeO_2/RGO oxide (20% wt). (d) comparing the degrdation efficiency in different conditions: in presence 1- Only ultrasound, 2- CdO/CeO_2 nanoparticles, 3- RGO and 4- CdO/CeO_2/RGO. (e) the changes in concentration (C_t/C_0) of IBP, RhB and MO {Reaction condition for all of comparing experiments: reactor volume for all of the experiments: 50 mL, initial concentration of MO and RhB 20 mg/L, reaction time: 150 min, pH=7.5, Initial concentration of IBP 20 mg/L in methanol, pH=4, $K_2S_2O_8$ 0.5 mmol/L: 1 mL reaction time: 80 min, catalyst amount (CdO/CeO_2 nanoparticles, RGO, CdO/CeO_2/RGO (20% wt): 1.2 g/L)}.

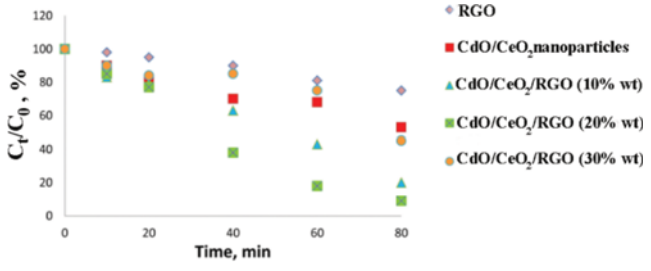

Fig. 5. The sonocatalytic degradation of IBP under ultrasonic irradiation. Experimental condition: reactor volume: 50 mL, initial concentration of IBP: 20 mg/L, ultrasonic power: 1,200 W/L, catalyst: 1.2 g/L, pH=4. $K_2S_2O_8$ (0.5 mmol/L): 1 mL.

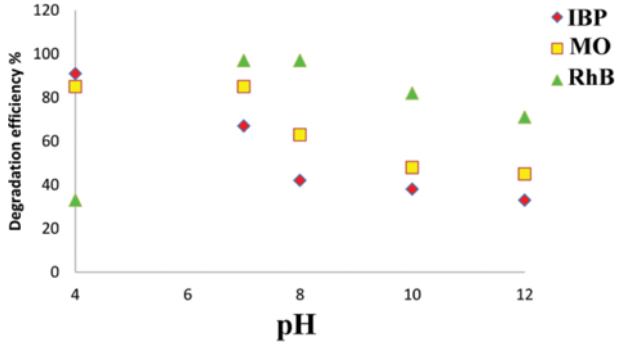

Fig. 6. Effect of pH values on degradation efficiency. Experimental condition: reactor volume: 50 mL, initial concentration of IBP, RhB and MO: 20 mg/L, ultrasonic power: 1,200 W/L, CdO/CeO_2/RGO (20 wt%): 1.2 g/L, $K_2S_2O_8$ (0.5 mmol/L)for IBP degradation: 1 mL.

sulfuric group, which is negatively charged in alkaline conditions. Because of high ^-OH in alkaline solution, there is weak interaction between MO molecules and CdO/CeO_2/RGO. That causes decreasing MO uptake. MO has highest degradation efficiency in neutral and acidic conditions. RhB has highest degradation efficiency at pH=7, 8. At pH value higher than 7, the existence of OH^- creates a competition between N^+-COO^-. It will decrease the aggregation of RhB, which causes an increase in the interaction of

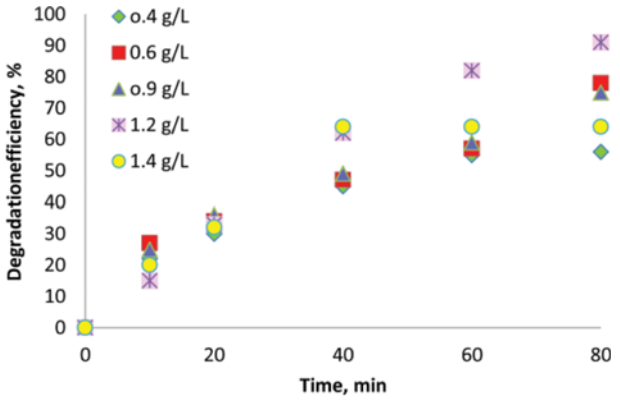

Fig. 7. Effect of dosage of catalyst on sonocatalytic reaction. Experimental condition: reactor volume: 50 mL, initial concentration of IBP: 20 mg/L, ultrasonic power: 1,200 W/L, CdO/CeO_2/RGO (20%wt): 1.2 g/L, pH=4, $K_2S_2O_8$ (0.5 mmol/L): 1 mL.

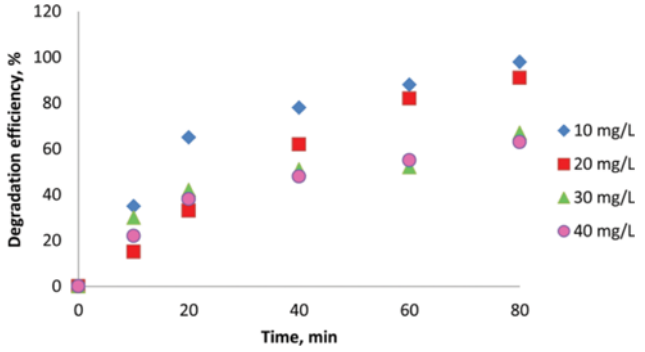

Fig. 8. Effect of initial concentration of IBP on sonocatalytic reaction. Experimental condition: reactor volume: 50 mL, CdO/CeO_2/RGO (20% wt): 1.2 g/L, ultrasonic power: 1,200 W/L pH=4, $K_2S_2O_8$ (0.5 mmol/L): 1 mL.

RhB with as-prepared nanocomposites. At pH higher than 8, with high ^-OH in alkaline solution, the electrostatic force of repulsion decreases the degradation efficiency.

To investigate other parameters on sonocatalytic reaction, degradation of IBP was chosen as a model reaction.

6. Effect of CdO/CeO_2/RGO Dosage

The dosage of the catalyst plays an important role in sonocatalytic degradation. Five different amounts of catalyst (0.3, 0.6, 0.9, 1.2 and 1.4 g/L) were considered. With increasing dosage of as-synthesized nanocomposites, the active sites of catalyst were increased. Thus, more radicals were produced and the degradation efficiency was increased. Fig. 7 presents the results of the experiments; the 1.2 g/L catalyst shows maximum removal efficiency (91%). However, with increase in the amount of catalyst (1.4 g/L), an increase in the particles aggregation occurs. In addition, the surface is not increasing in a geometrical ratio. Therefore, the number of active sites on the catalyst decreased and ultrasonic wave penetration decreased. Consequently, degradation efficiency decreased. Subsequent experiments were performed using sonocatalyst dosage of 1.2 g/L as optimal value.

7. Effect of Initial Concentration of Organic Pollutant

To study the effects of initial concentration of organic pollutant on sonocatalytic reaction, four different amounts of initial concentration of IBP (10, 20, 30 and 40 mg/L) were considered. Fig. 8 shows that with increasing the initial concentration of IBP, the number of the IBP is increased, whereas the number of hydroxyl radicals is constant. More hydroxyl radicals are required for degradation of all of the molecules; therefore, the degradation efficiency is decreased. The results show initial concentration of IBP (20 mg/L) is suitable.

8. Effect of Ultrasonic Power

To study the effects of output power of ultrasound in experiments, degradation of IBP was studied in two different outputs (500 W, 1,200 W). The results indicate that when output power of apparatus is increased from 500 W to 1,200 W, degradation efficiency is increased. With applying 1,200 W output power, acoustic cavitation phenomenon is more rapid and more hydroxyl radicals are produced; thus, degradation efficiency is increased (Fig. S3 in supplementary materials).

9. Mechanism of Sonocatalytic Reaction

Ultrasound irradiation leads to acoustic cavitation (the forma-

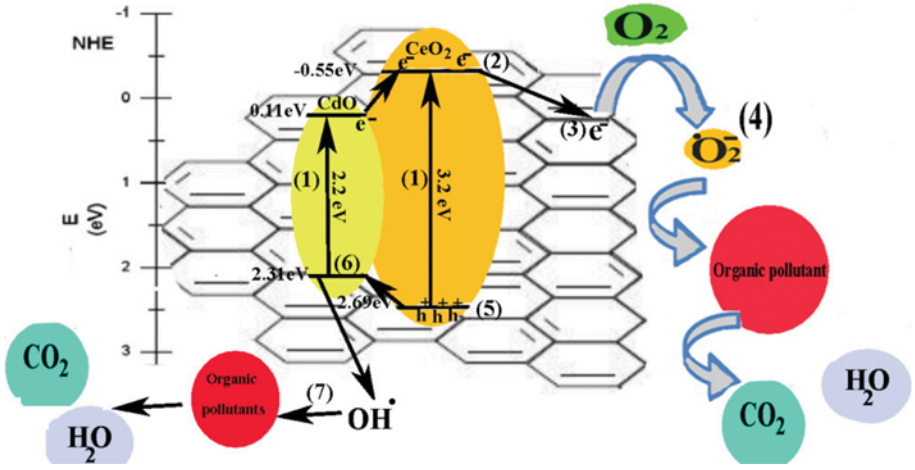

Fig. 9. Sonocatalytic degradation mechanism for the organic pollutants over CdO/CeO_2/RGO under ultrasonic irradiation.

tion, growth and collapsing bubbles) consisting of hotspots that can cause pyrolysis of water. This process can result in the formation of reactive radicals such as $^{\bullet}H$ and $^{\bullet}OH$ (Eq. (3)). Furthermore, some additional consecutive chain reactions can be happen as shown in Eqs. (4)-(8). According to many studies, the presence of reactive radicals such as $^{\bullet}H$ and $^{\bullet}OH$ can enhance the oxidizing power of ultrasonication and provide additional nuclei; this process can increase the rate of formation of cavitation bubbles and increase the generation of hydroxyl radicals [41,42]. Ultrasonic irradiation has many advantages; however, complete minimization of the organic pollutant via ultrasonication alone needs high reaction time and large amount of energy (see Fig. 4(d). To overcome these problems, degradation with ultrasonication can be improved by adding a suitable catalyst to accelerate the reaction. Fig. 9 illustrates the electron transfer mechanism in the sonocatalytic degradation of the organic pollutants. When CdO/CeO_2/RGO is irritated by ultrasonication, both CdO and CeO_2 semiconductors are excited and the electrons are excited from the valence band to conduction band, forming electron-holes pairs [43-46]. The band gap of CdO/CeO_2/RGO is calculated from the equation,

$$(\alpha h\nu)^2 = K(h\nu - E_g) \quad (2)$$

where $h\nu$ is the energy of a photon, α is the absorption coefficient, K is a constant and E_g is the band gap [47]. With diffuse reflectance spectra (DRS) the band gap of CdO/CeO_2/RGO can be determined by extrapolating the linear region in a diagram of $(\alpha h\nu)^2$ against the photon energy. Through this method, the band gap energy of CdO/CeO_2/RGO is obtained 1.75 ev (Fig. S4). The energy level differences between RGO, CeO_2 and CdO are in favorable positions to promote an effective charge separation, retarding the charge recombination.The conduction bands of CdO and CeO_2 are very close together; electrons are injected from the conduction band of CdO into the conduction band of CeO_2. This process can lead to high concentration of electrons in the conduction band of CeO_2 and charge separation. Afterwards, the electrons can easily transfer to RGO due to the good conductivity of RGO, which can effectively improve the separation of sonogenerated e^--h^+ pairs enhancing the efficiency of the sonocatalytic degradation. The electrons can combine with O_2 in solution to form the strong oxidative species $^{\bullet}O_2^-$; on the other hand, some of the excited holes at the valence band of CeO_2 would transfer to the valence band of the CdO via graphene. The h^+ can react with surface adsorbed H_2O to produce $^{\bullet}OH$ radical or directly oxidize organic pollutants to CO_2, H_2O and some other small molecules (Eqs. (9)-(16)).

Note that the removal efficiency of IBP remarkably increases from 44% to 91% in the presence $K_2S_2O_8$. The $S_2O_8^{-2}$ reacts with the conduction band electrons and generates $^{\bullet}SO_4^-$. Subsequently, the produced sulfate radicals can lead to the production of $^{\bullet}OH$. Since, the standard redox potential of $^{\bullet}SO_4^-$ (E=3.17 ev) is higher than hydroxyl radical (E=2.72 ev). The removal efficiency of IBP is notably increased in presence of $K_2S_2O_8$.

To further understand the sonocatalytic mechanism, trapping experiments using L-His, thiore and VC as the quenching agents were carried out to determine the main reactive oxidant species. Fig. S5 clearly displays the addition of effective reducers. In general, L-Histidine can quench the singlet molecular oxygen ($^1O_2$) and $^{\bullet}OH$, Thiourea quenches the hydroxyl radical ($^{\bullet}OH$), and Vitamin C can quench most kinds of radicals [48,49].

As can be seen in Fig. S5, with CdO/CeO_2/RGO and ultrasonication, the absorbance of DPCO at 563 nm decreased by 58%, 83% and 91% in presence of L-His, Thiourea and Vitamin C (VC), respectively. Utilization of these scavengers inhibits to produce $^1O_2$ and $^{\bullet}OH$ radicals. Thus absorbance of DPCO is decreased. It is found that $^{\bullet}OH$ and $^1O_2$ are major kinds of ROS with ultrasonic irradiation. Based on the above results, the mechanisms of ultrasonic wave's absorption, charge transfer, and the reaction pathways are as follows:

$$H_2O + \text{ultrasound} \rightarrow {}^{\bullet}OH + H^{\bullet} \quad (3)$$

$$^{\bullet}OH + H^{\bullet} \rightarrow H_2O \quad (4)$$

$$^{\bullet}OH + {}^{\bullet}OH \rightarrow H_2O_2 \quad (5)$$

$$H_2O_2 + H^{\bullet} \rightarrow H_2O + {}^{\bullet}OH \quad (6)$$

$$H^{\bullet} + O_2 \rightarrow HO_2^{\bullet} \quad (7)$$

$$HO_2^{\bullet} + HO_2^{\bullet} \rightarrow H_2O_2 + O_2 \quad (8)$$

$$\text{ultrasound} \rightarrow h\nu \quad (9)$$

$$CdO/CeO_2 + \text{ultrasound irradiation} \rightarrow CdO/CeO_2(e^- + h^+) \quad (10)$$

$$CdO/CeO_2(e^-) + RGO \rightarrow CdO/CeO_2 + RGO(e^-) \quad (11)$$

$$e^- + h^+ \rightarrow \text{heat or hv} \quad (12)$$

$$h^+ + H_2O \rightarrow {}^{\bullet}OH + H^+ \quad (13)$$

$$e^- + O_2 \rightarrow {}^{\bullet}O_2^- \quad (14)$$

$$^{\bullet}O_2^- + \text{Organic pollutants} \rightarrow CO_2 + H_2O + \text{product} \quad (15)$$

$$^{\bullet}OH + \text{Organic pollutants} \rightarrow CO_2 + H_2O + \text{product} \quad (16)$$

10. Catalytic Reduction of 4-NP to 4-AP

To study the catalytic properties of CdO/CeO_2/RGO, the reduction of 4-NP by $NaBH_4$ was carried out. Fig. 10 shows the UV-Vis spectra of 4-NP solution from 250 to 500 nm at intervals of 15 min, using CdO/CeO_2/RGO as catalyst and $NaBH_4$ as reductant. It is

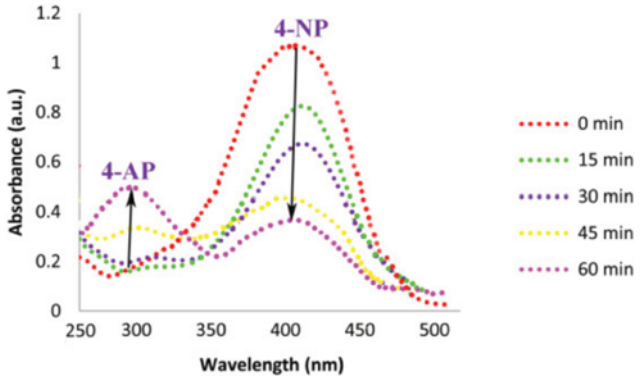

Fig. 10. UV-vis spectra of 4-NP in presence $NaBH_4$ (catalytic reaction). 4-NP reaction condition: deionized water (100 mL), (5 mM) 4-NP solution (2 mL), CdO/CeO_2/RGO: 1.2 g/L, $NaBH_4$ (0.1 M): 2 mL.

clear that the maximum absorption peak of 4-NP is at 400 nm. The 4-AP has a strong absorption peak at 300 nm. As the reaction proceeds, due to conversion of 4-NP to 4-AP, the maximum absorption peak at 400 nm gradually decreases and a new peak at 300 nm slowly appears. Thus, the concentration of the 4-NP solution is decreased and 4-AP concentration is increased. The results indicate that the reduction efficiency at 60 min after the beginning of the reaction is 79%.

11. Mechanism of 4-NP Reduction to 4-AP

The reduction of 4-NP by the CdO/CeO_2/RGO catalyst can be explained by Langmuir-Hinshelwood model. 4-NP is initially adsorbed on the CdO/CeO_2 surface and then BH_4^- ions donate the electrons to CdO/CeO_2. Further, the CdO/CeO_2 transfers these electrons to 4-NP, resulting in the reduction of 4-NP at the surface of CdO/CeO_2 nanoparticles. In this reaction BH_4^- acts as electron donor as well as hydrogen supplier. The reduction efficiency in presence of CdO/CeO_2 nanoparticles after the end of 60 min is 45%. It is noticed that reduction efficiency after the end of 60 min is 55% in the presence of RGO. This is due to (1) High adsorption ability of the RGO; (2) Strong π-π interactions with the 4-NP; and (3) Slow electron recombination. The highest reduction efficiency is achieved by CdO/CeO_2/RGO. It implies that with synergistic effect of nanoparticles and graphene, BH_4^- ions adsorption and decomposition is fast. BH_4^- ions easily adsorb on the surface of nanoparticles. Easy transfer of electrons from one semiconductor to another occurs. RGO also plays its own role and provides the support for 4-NP, with transferring a surface hydrogen species to the surface of 4-NP, which is adsorbed and easily reduces it into 4-AP. In the next step, product 4-AP desorbs and leaves the catalyst surface.

Fig. 11 shows the removal efficiency of CdO/CeO_2/RGO in the optimized condition. For sonocatalytic reaction at the end of 80 min, 91% of IBP and at the end of 150 min 85% of MO, 97% of RhB were degraded. The removal efficiency increased almost linearly with increasing time irradiation. In catalytic reaction with $NaBH_4$, the reduction efficiency of 4-NP is 79% at the end of 60 min.

12. Kinetic Study of the Catalytic and Sonocatalytic Reactions

Fig. S6 shows that by increasing the concentration of $NaBH_4$ up to 0.1 M, the rate of 4-NP reduction is increased and it remains constant after 0.1 M. The kinetics of 4-NP reduction in presence

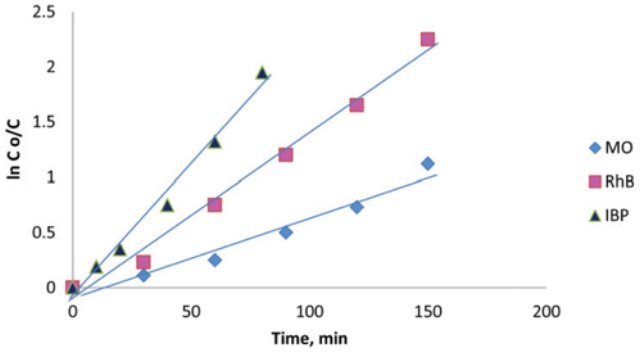

Fig. 12. The reaction kinetic plot for sonocatalytic degradation of MO and RhB. The pseudo-first order kinetics ($-dC/dt = k_{app}C$).

Table 1. Rate coefficient of sonocatalytic degradation of MO, RhB, IBP and catalytic reduction of 4-NP

Experimental conditions	k_{app} (min^{-1})	R^2
CdO/CeO_2/RGO, Ultrasonic, MO	7.34×10^{-3}	0.97
CdO/CeO_2/RGO, Ultrasonic, RhB	2×10^{-2}	0.98
CdO/CeO_2/RGO, Ultrasonic, IBP	1.12×10^{-2}	0.99
CdO/CeO_2/RGO, Ultrasonic, 4-NP	1.32×10^{-2}	0.98

CdO/CeO_2/RGO was studied with varying catalyst dosage from 0.6-1.4 g/L, keeping other parameters constant (0.1 M $NaBH_4$, 5×10^{-3} M 4-NP). With increasing amount of CdO/CeO_2/RGO, the rate constant enhances up to 1.2 g/L and then it remains almost constant (Fig. S7). Therefore, the rate of the reduction greatly depends on concentration of $NaBH_4$ and concentration of CdO/CeO_2/RGO. Due to large excess of $NaBH_4$ relative to 4-NA, the $NaBH_4$ concentration can be considered as a constant, so the reduction could be assumed first order. The plot of ln C_0/C of 4-NP vs reaction time is almost linear and 4-NP reaction is pseudo-first-order kinetics ($k_{app}=1.32\times10^{-2}$). In sonocatalytic reactions, all calculated $\ln C_0/C$ values were approximately linear with irradiation time as presented in Fig. 12. Therefore, the sonocatalytic degradation of IBP, MO and RhB obeys first-order reaction kinetics. The

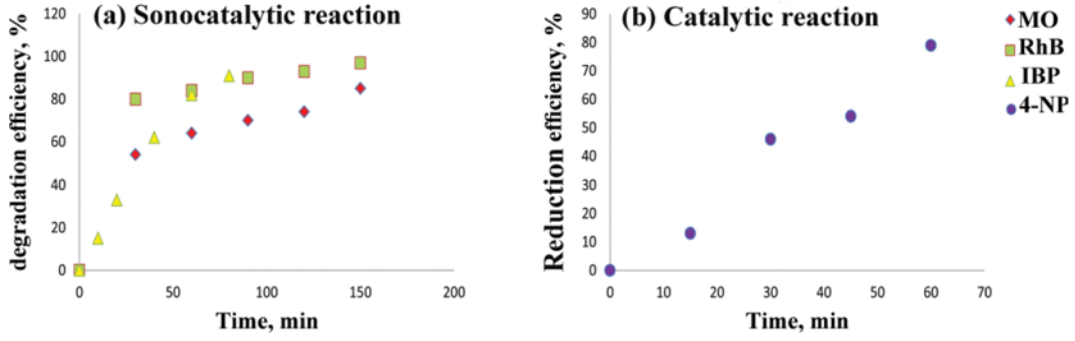

Fig. 11. Removal efficiency of (a) IBP, MO, RhB in sonocatalytic reaction and (b) 4-NP in catalytic reaction. MO and RhB reaction condition: MO and RhB (20 mg/L): 25 mL, pH=7.5, CdO/CeO_2/RGO: 1.2 g/L,ultrasonic power: 1,200 W/L, IBP (20 mg/L): 25 mL, pH=4, CdO/CeO_2/RGO: 1.2 g/L, ultrasonic power: 1,200 W/L, $K_2S_2O_8$ (0.5 mmol/L): 1 mL. 4-NP reaction condition: deionized water (100 mL), (5 mM) 4-NP solution (2 mL), CdO/CeO_2/RGO: 1.2 g/L, $NaBH_4$ (0.1 M): 2 mL.

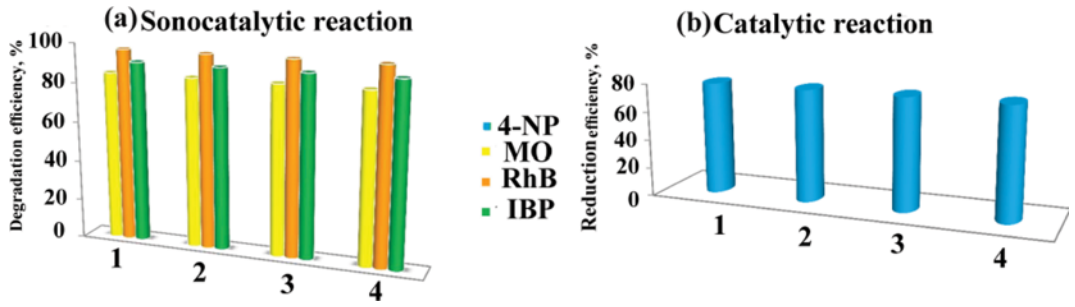

Fig. 13. Removal efficiency of recycled CdO/CeO_2/RGO (a) in sonocatalytic reaction and (b) in catalytic reaction. Reaction condition: the cleaned CdO/CeO_2/RGO were immersed in ethanol for 6 h and rinsed with deionized water and then dried at 70 °C. MO and RhB (20 mg/L): 25 mL, pH=7.5, CdO/CeO_2/RGO: 1.2 g/L, ultrasonic power: 1,200 W/L. IBP (20 mg/L): 25 mL, pH=4, CdO/CeO_2/RGO: 1.2 g/L, ultrasonic power: 1,200 W/L, $K_2S_2O_8$ (0.5 mmol/L): 1 mL. 4-NP reaction condition: deionized water (100 mL), (5 mM) 4-NP solution (2 mL), CdO/CeO_2/RGO: 1.2 g/L, $NaBH_4$ (0.1 M): 2 mL.

k_{app} of rate of reduction and degradation of 4-NP, MO and RhB are listed in Table 1.

13. The Reusability Test

The level of stability and reusability of the catalysts is an important factor for practical applications. To evaluate stability of CdO/CeO_2/RGO, it was reused for four times in sonocatalytic and catalytic reactions separately. From Fig. 13 it is obvious that after four times the degradation and reduction efficiency is constant, indicating the excellent stability of as-prepared nanocomposite.

CONCLUSION

CdO/CeO_2/RGO was synthesized with simple hydrothermal method. The presented synthesis is simple, efficient and low cost. CdO/CeO_2/RGO was characterized by FTIR, XRD, DRS, SEM and EDX. We evaluated CdO/CeO_2/RGO in sonocatalyst and catalytic reaction. In the sonocatalytic reaction, using ultrasonic waves and CdO/CeO_2/RGO together, the highest degradation efficiency of IBP (91%) in presence $K_2S_2O_8$, RhB (97%) and MO (85%) was observed at a certain time after beginning the reaction. In catalytic reaction, the highest reduction efficiency of 4-NP took place at 60 min after beginning the reaction (79%). Reusability experiments were conducted and showed very little change in removal efficiency, which indicates the stability of the as-prepared catalyst. All optimizing the experiments occurred in dark condition. It proves the reduction and degradation of 4-NP, IBP and azo dyes (MO and RhB) requires no additional irradiation with visible or UV light. This characteristic can prove to be beneficial for practical applications.

ACKNOWLEDGEMENT

Support of this investigation by Alzahra University is gratefully acknowledged.

SUPPORTING INFORMATION

Additional information as noted in the text. This information is available via the Internet at http://www.springer.com/chemistry/journal/11814.

REFERENCES

1. Y. Tu, C. You, C. Chang and S. Wang, *Chem. Eng. J.*, **225**, 433 (2013).
2. Y. Jiang, Y. Sun, H. Liu, F. Zhu and H. Yin, *Dyes Pigm.*, **78**, 77 (2008).
3. S. Merouani, O. Hamdaoui, F. Saoudi and M. Chiha, *Chem. Eng. J.*, **158**, 550 (2010).
4. A. Z. Abdullah and P. Y. Ling, *J. Hazard. Mater.*, **173**, 159 (2010).
5. K. B. Narayanan and N. Sakthivel, *Bioresour. Technol.*, **102**, 10737 (2011).
6. I. Georgaki, E. Vasilaki and N. Katsarakis, *Am. J. Anal. Chem.*, **5**, 518 (2014).
7. X. Lu, B. Yang, J. Chen and R. Sun, *J. Hazard. Mater.*, **161**, 241 (2009).
8. J. V Castell, M. A. Miranda and I. M. Morera, *Photo Chem. Photobiol.*, **38**, 991 (1987).
9. H. Gong, W. Chu, S. Hiu and A. Y. Lin, *Chemosphere.*, **167**, 415 (2017).
10. G. Ca, P. Valeria, P. Brunella and C. Sergio, *J. Pharm Biomed Anal.*, **30**, 499 (2002).
11. J. Madhavan, P. Maruthamuthu, S. Murugesan and S. Anandan, *Appl. Catal. C: Environ.*, **83**, 8 (2008).
12. A. Ziylan, S. Dogan, S. Agopcan and R. Kidak, *Environ. Sci. Pollut. Res.*, **21**, 5929 (2014).
13. J. Wang, Y. Lv, L. Zhang, B. Liu, R. Jiang and G. Han, *Ultrason. Sonochem.*, **17**, 642 (2010).
14. W. Zhang, X. Xiao, T. An, Z. Song, J. Fu, G. Sheng and M. Cui, *J. Chem. Technol. Biotechnol.*, **78**, 788 (2003).
15. P. Chartrin, *Environ. Sci. Technol.*, **34**, 3474 (2000).
16. B. Naik, S. Hazra, V. S. Prasad and N. N. Ghosh, *Catal. Commun.*, **12**, 1104 (2011).
17. D. Rawtani and Y. K. Agrawal, *Rev. Adv. Mater. Sci.*, **30**, 282 (2012).
18. S. Naraginti, F. Bernard, A. Radhakrishnan and A. Sivakumar, *Spectrochim. Acta. Part A Mol. Biomol. Spectrosc.*, **135**, 814 (2015).
19. S. Chianese, P. Iovino, S. Canzano, M. Prisciandaro, S. Chianese, P. Iovino, S. Canzano and M. Prisciandaro, *Desalin. Water Treat.*, **3994**, 1 (2016).
20. Z. Lei, J. Wang, L. Wang, X. Yang, D. Pan, G. Xu and L. Tang, *J. Hazard. Mater.*, **312**, 298 (2016).

21. Z. H. U. Lei, T. Ghosh, C. Park, M. Zeda and O. H. Won-chun, *Chinese J. Catal.*, **33**, 1276 (2012).
22. M. Ahmad, E. Ahmed, Z. L. Hong, W. Ahmed, A. Elhissi and N. R. Khalid, *Ultrason. Sonochem.*, **21**, 761 (2014).
23. S. Thangavel, N. Raghavan, G. Kadarkarai, S. Kim and G. Venugopal, *Ultrason. Sonochem.*, **24**, 123 (2015).
24. P. Saharan, G. Ram, S. Lata, S. K. Mehta and S. Mor, *Ultrason. Sonochem.*, **22**, 317 (2015).
25. S. Lin and H. Weng, *Appl. Catal. A.*, **118**, 21 (1994).
26. D. Chang, I. Chen, M. Chen and S. Lin, *Chemosphere.*, **52**, 943 (2003).
27. S. K. Bhargava, J. Tardio, J. Prasad, K. Fo, D. B. Akolekar and S. C. Grocott, *Ind. Eng. Chem. Res.*, **45**, 1221 (2006).
28. H. Li, X. Gui, C. Ji, P. Li, Z. Li, L. Zhang, E. Shi, K. Zhu and J. Wei, *Nano Res.*, **5**, 265 (2012).
29. T. Xu, L. Zhang, H. Cheng and Y. Zhu, *Appl. Catal. B: Environ.*, **101**, 382 (2011).
30. B. N. Joshi, H. Yoon, S. Na, J. Choi and S. S. Yoon, *Ceram. Int.*, **40**, 3647 (2014).
31. A. Priyadharsan, V. Vasanthakumar, S. Karthikeyan, V. Raj, S. Shanavas and P. M. Anbarasan, *J. Photochem. Photobiol. A Chem.*, **346**, 32 (2017).
32. S. Shanavas, A. Priyadharsan, V. Vasanthakumar, A. Arunkumar, P. M. Anbarasan and S. Bharathkumar, *J. Photochem. Photobiol. A Chem.*, **340**, 96 (2017).
33. M. Lashanizadegan and H. Mirzazadeh, *J. Ceram. Process. Res.*, **13**, 389 (2012).
34. X. Zhu, Y. Zhu, S. Murali, M. D. Stoller and R. S. Ruoff, *ACS Nano.*, **5**, 3333 (2011).
35. P. K. Sahoo, B. Panigrahy and D. Bahadur, *RSC Adv.*, **4**, 48563 (2014).
36. P. V. Kamat, *Chem. Rev.*, **93**, 267 (1993).
37. A. F. De Faria, D. S. T. Martinez, S. M. M. Meira, A. C. M. de Moraes, A. Brandelli, A. G. S. Filho and O. L. Alves, *Colloids Surf., B.*, **113**, 115 (2014).
38. M. Farahmandjou and M. Zarinkamar, *Mater.*, **48**, 5 (2015).
39. S. Oh, W. S. Shin and H. T. Kim, *Environ. Sci. Pollut. Res.*, **23**, 22882 (2016).
40. J. Paul (Guin), D. B. Naik, Y. K. Bhardwaj and L. Varshney, *Radiation Phys. Chem.*, **100**, 38 (2014).
41. N. H. Ince, G. Tezcanli, R. K. Belen and G. Apikyan, *Appl. Catal. B Environ.*, **29**, 167 (2001).
42. S. N. Nam, S. K. Han, J. W. Kang and H. Choi, *Ultrason. Sonochem.*, **10**, 139 (2003).
43. A. E. Raevskaya, A. L. Stroyuk and S. Y. Kuchmiy, *J. Colloid Interface Sci.*, **302**, 133 (2006).
44. K. R. Murali, V. Swaminathan and D. C. Trivedi, *Sol. Energy Mater. Sol. Cells.*, **81**, 113 (2004).
45. R. W. Matthews, *J. Phys. Chem.*, **91**, 3328 (1987).
46. C. Petrier, A. Jeunet, J.-L. Luche and G. Reverdy, *J. Am. Chem. Soc.*, **114**, 3148 (1992).
47. M. Kaur, K. P. Muthe, S. K. Despande, S. Choudhury and J. B. Singh, *J. Cryst. Growth*, **289**, 670 (2006).
48. C. Xiao-jun, X. U. Han-hong, W. Yu-jian, H. U. Shan, Z. Zhi-xiang and Z. Yao-mou, *Agric. Sci. China*, **6**, 458 (2007).
49. S. ichiro Umemura, N. Yumita, K. Umemura and R. Nishigaki, *Cancer Chemother. Pharmacol.*, **43**, 389 (1999).

Supporting Information

Binary semiconductor oxide nanoparticles on graphene oxide (CdO/CeO_2/RGO) for the treatment of hazardous organic water pollutants

Hoda Mirzazadeh and Maryam Lashanizadegan[†]

Department of Chemistry, Faculty of Physics & Chemistry, Alzahra University, P. O. Box 1993893973, Tehran, Iran
(*Received 29 July 2017 • accepted 22 October 2017*)

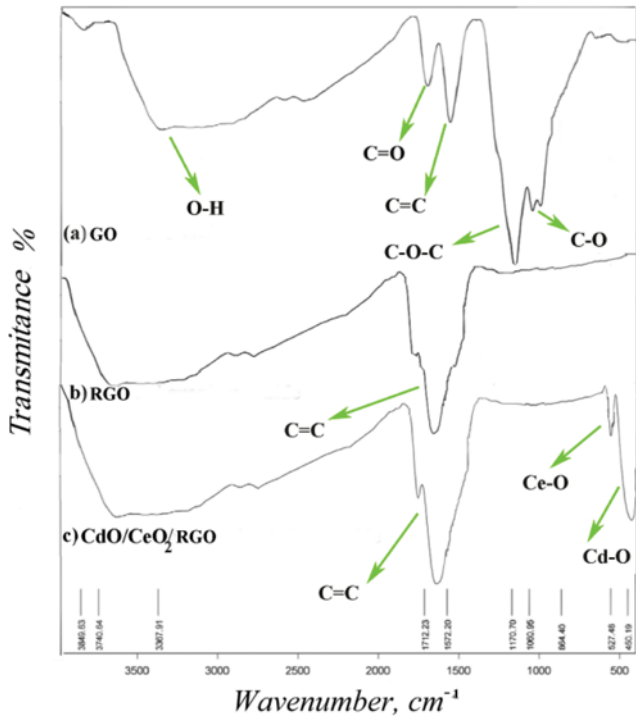

Fig. S1. FTIR spectra of (a) GO, (b)RGO, (c) CdO/CeO_2/RGO.

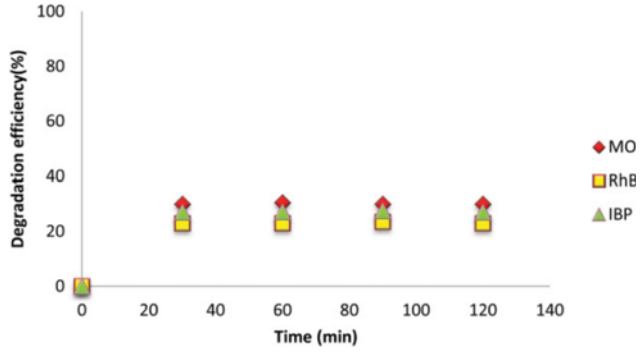

Fig. S2. Percentage removal of the organic pollutants without ultrasonic (adsorption study).

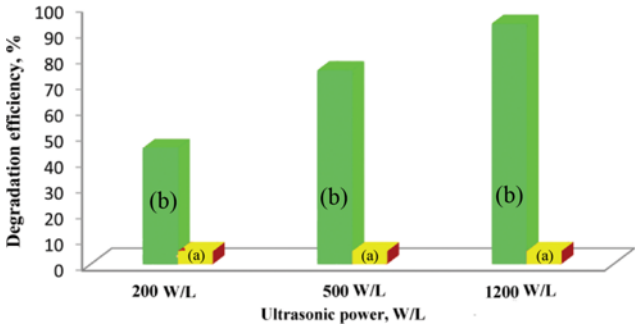

Fig. S3. Effect of ultrasonic output power to degradation IBP. Experimental condition: CdO/CeO_2/RGO (20% wt): 1.2 g/L, initial concentration of IBP: 20 mg/L pH=4, $K_2S_2O_8$ (0.5 mmol/L): 1 mL.

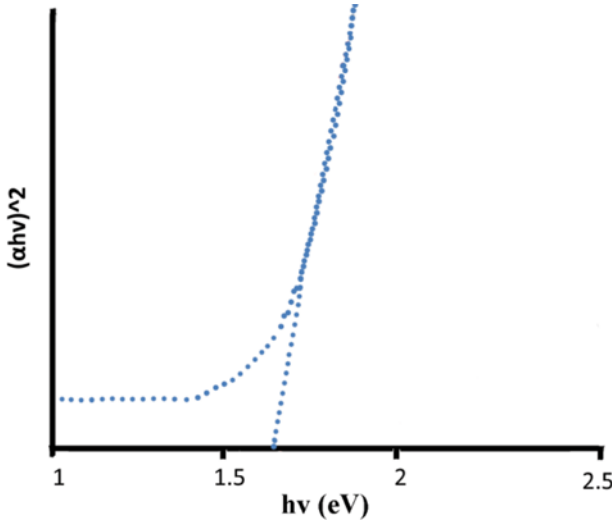

Fig. S4. $(\alpha h\nu)^2 - h\nu$ curve of CdO/CeO_2/RGO.

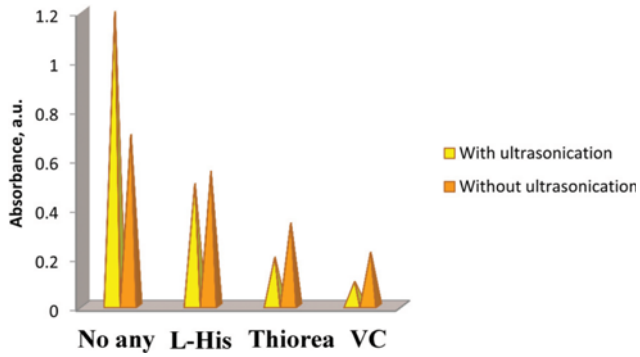

Fig. S5. Absorbance of DPCO in DPCI+as-prepared nanocomposites solutions in the presence of various quenching reagents. Experimental condition: with and without ultrasonic irradiation, ([DPCI]=10^{-2} M, [CdO/CeO_2/RGO (20% wt)]=1.2 g/L, [His]=[VC]=[Thiourea]=5.0×10^{-3} M and US power= 1,200 W/L Ultasounic time: 45 min.

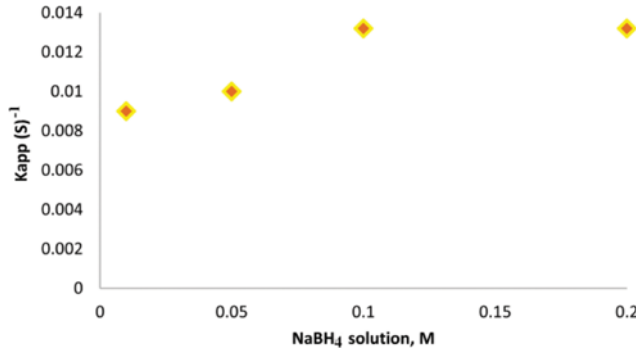

Fig. S6. Effect of $NaBH_4$ concentration on catalytic reduction of 4-NP in presence of CdO/CeO_2/RGO. Reaction condition: deionized water (100 mL), (5 mM) 4-NP solution (2 mL), CdO/CeO_2/RGO: 1.2 g/L.

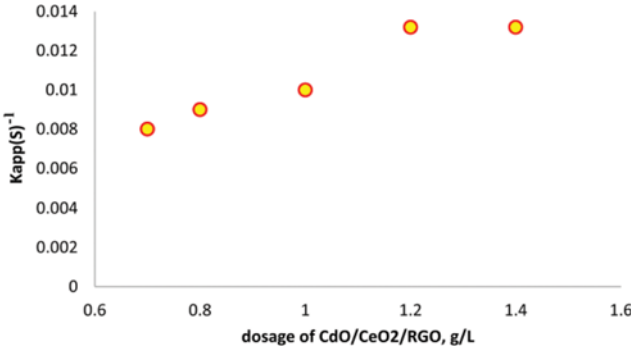

Fig. S7. Effect of dosage of CdO/CeO_2/RGO on reduction of 4-NP. Reaction condition: deionized water (100 mL), (5 mM) 4-NP solution (2 mL), $NaBH_4$ (0.1 M): 2 mL.